

Cherenkov Telescope Array Observatory sensitivity to heavy Galactic Cosmic Rays and the shape of particle spectrum

C. Dubos,^{a,1} P. Sharma,^{a,b} S. Patel^{a,2} and T. Suomijärvi^a

^aUniversité Paris-Saclay, CNRS/IN2P3, IJCLab,
91405 Orsay, France

^bUniversité de Strasbourg, CNRS, Observatoire astronomique de Strasbourg, UMR 7550,
F-67000 Strasbourg, France

E-mail: coline.dubos@ijclab.in2p3.fr, pooja.sharma@unistra.fr,
tiina.suomijarvi@ijclab.in2p3.fr

Abstract. The origin of Galactic Cosmic Rays (GCRs) and the potential role of Supernova Remnants (SNRs) as cosmic-ray (CR) accelerators remain subjects of ongoing debate. To shed more light on this topic, we have studied the spectral **shapes** of two SNRs, RX J1713.7-3946 and HAWC J2227+610, performing simulations for the Cherenkov Telescope Array Observatory (CTAO). The previous multi-wavelength (MWL) analysis on these two sources showed an important hadronic contribution at high energies. The interaction of the GCRs accelerated by the SNRs with the medium around the accelerator leads to a process of pion decay (PD) that produces gamma-rays (γ -rays). These emissions, detectable by CTAO, offer an indirect means of pinpointing the CR source.

Two scenarios have been considered: the contribution of heavy CRs and different cut-off sharpnesses (β) of the particle spectra. The simulations were performed by using different CR composition distributions (protons, CNO, Fe) and different sharpness values ranging from $\beta=0.5$ to $\beta=1.5$.

The results show that, in the cases studied here, CTAO will increase the sensitivity to the spectral shape of γ -rays. This allows us to distinguish protons from heavy CRs and obtain information on β values and therefore on different acceleration scenarios.

Keywords: cosmic ray experiments, gamma ray detectors, supernova remnants

¹Corresponding author.

²Also at Helmholtz-Zentrum Berlin für Materialien und Energie.

Contents

1	Introduction	1
2	Selection of the SNR sources	3
2.1	MWL study of Galactic SNRs	3
2.2	The selected sources	3
2.2.1	RX J1713.7-3946	3
2.2.2	HAWC J2227+610	3
3	Evolution of the particle spectrum	4
3.1	Composition of the CRs	4
3.2	Acceleration models	5
4	Modelling and simulation of the γ-ray spectra for CTAO	6
4.1	Modelling with GAMMAPY	6
4.2	γ -ray spectrum modelling	6
4.2.1	Particle spectrum by SNR	6
4.2.2	γ -ray spectrum from the π^0 decay process	7
4.3	CTAO γ -ray spectrum simulation	9
4.3.1	Simulating with GAMMAPY	9
4.3.2	Input parameters for simulations	10
4.3.3	Data fitting and likelihood test	12
5	Results	12
5.1	CTAO sensitivity to heavy nuclei	12
5.2	CTAO sensitivity to different proton acceleration models	13
5.3	CTAO sensitivity to separate heavy nuclei and proton acceleration models	13
5.4	Contribution of electrons	17
6	Conclusions	18

1 Introduction

For over a century, direct and indirect observations have provided detailed information on the energy spectrum of CRs. This spectrum spans an impressive range of 12 orders of magnitude in energy and 32 in flux. A pronounced softening of the CR spectrum is observed at around 3×10^{15} eV. This so-called knee is attributed to light CR primaries (such as protons) [1]. A less pronounced second knee attributed to heavy primaries (such as Fe), is observed at around 9×10^{16} eV [2, 3] and a mixed composition is observed between these two energies.

The CRs below 10^{18} eV are believed to be accelerated by Galactic sources. Above this energy, the sources are shown to be extragalactic [4]. The identification of Galactic sources that can accelerate CRs up to the knee energies, also known as PeVatrons, remains an active field of research. Supernova (SN) explosions are among the most violent high-energy phenomena in our Galaxy and their remnants (SNRs) emerge as one of these potential Galactic sources with an energy budget sufficient to

accelerate CRs up to the PeV energy [5] (and references therein). Approximately 10-20 per cent of the kinetic energy from a SN explosion is converted into accelerated particles through diffusive shock acceleration (DSA) [6, 7]. If one supposes three SN explosions per century in the Milky Way, the energy budget would be sufficient to reproduce the CR spectrum.

After being accelerated by SNR shock waves, CRs **could** escape from the remnant and interact with the surrounding medium. This can lead to emission of high-energy γ -rays through the inelastic production of neutral pions π^0 in proton-proton collisions:

$$\begin{cases} p + p \rightarrow \pi^0 + p + p \\ \pi^0 \rightarrow 2\gamma \end{cases} \quad (1.1)$$

The γ -rays emitted in opposite directions have an energy of ~ 70 MeV in the π^0 rest frame. The threshold energy (kinetic energy of a proton colliding with another stationary proton) for π^0 production is 280 MeV. Therefore, the γ -rays from the π^0 decay have a typical signature in the spectrum called "pion-decay bump" [8]. The identification of the "pion-decay bump" would allow us to sign the underlying hadronic interactions. γ -rays, which are neutral messengers, travel in a straight line through the Galaxy until they reach Earth. In contrast, charged CRs are deviated by Galactic magnetic fields and lose the knowledge of their original **directions**. Therefore, the observation of these γ -rays allows us to point back to the source of the hadronic interaction and, consequently, to the CR accelerator.

In addition to the PD-component, high-energy γ -rays are also produced by electrons through synchrotron, bremsstrahlung, and inverse Compton (IC) processes. The various processes can be identified by using multi-wavelength (MWL) analysis. In a recent study by [9], such MWL analysis was performed for several Galactic SNRs. An important hadronic contribution was observed for many of them, in particular for RX J1713.7-3946 and HAWC J2227+610. These sources were selected to be the objects of this study.

High-energy γ -rays interact with the atmosphere, generating cascades of particles inducing Cherenkov light. This light can be detected by ground-based Cherenkov telescopes. The current generation of Imaging Atmospheric Cherenkov Telescopes (IACTs) such as H.E.S.S. [10], the Major Atmospheric Gamma-Ray Imaging Cherenkov telescopes (MAGIC) [11] and the Very Energetic Radiation Imaging Telescope Array System (VERITAS) [12] have provided a wealth of information on objects emitting high-energy γ -rays. Currently, the next generation instrument Cherenkov Telescope Array Observatory (CTAO) is being constructed [13]. CTAO will consist of more than 100 telescopes, distributed between two sites: La Palma (Canary Island), in the northern hemisphere, and near the Cerro Paranal Observatory in Chile, in the southern hemisphere, thereby covering the entire night sky. CTAO will cover γ -ray energies from 20 GeV to 300 TeV, thanks to its three types of telescopes: the Small-Sized Telescope (SST), the Medium-Sized Telescope (MST) and the Large-Sized Telescope (LST). In its Alpha configuration, that includes 14 MSTs and 37 SSTs in the southern site and 4 LSTs, and 9 MSTs in the northern site, CTAO will provide an energy resolution below 10% for energies larger than 1 TeV, an angular resolution better than 0.1° , and a sensitivity 10 times greater than its predecessors.

The goal of this paper is to study the potential of CTAO to distinguish protons from heavy CRs through observations of γ -rays and to obtain information on different hadronic acceleration scenarios. Two SNRs have been considered: RX J1713.7-3946 and HAWC J2227+610. To achieve this, we have considered different compositions of GCRs and different shapes of particle distributions predicted

by acceleration models. Simulations for CTAO were performed by using radiative models with the parameters obtained by the MWL study [9].

2 Selection of the SNR sources

2.1 MWL study of Galactic SNRs

The MWL analysis of 9 Galactic SNRs was realized by [9]. This analysis assumed that the observed spectral energy distribution (SED) was due to the synchrotron, bremsstrahlung, IC and PD processes. A lepto-hadronic (synchrotron, bremsstrahlung, IC and PD processes) scenario, and a pure leptonic scenario (synchrotron, bremsstrahlung, IC processes) were taken into consideration to model the observed flux. Based on a likelihood comparison between the pure leptonic and lepto-hadronic scenarios, it was shown that the γ -ray spectra of RX J1713.7-3946 and HAWC J2227+610 were more accurately reproduced when the lepto-hadronic scenario with a predominant hadronic contribution at high energies, was considered. Moreover, at an energy of 100 TeV, RX J1713.7-3946 has a flux of 5×10^{-12} erg cm $^{-2}$ s and HAWC J2227+610 has a flux of 5×10^{-13} erg cm $^{-2}$ s, both of which are above the CTAO sensitivity (for an observation duration of 50 hours).

2.2 The selected sources

2.2.1 RX J1713.7-3946

RX J1713.7-3946 (also known as **HESS J1713-397**, radio designation G347.3-0.5) is the most-studied young γ -ray shell SNR [14]. It was discovered in the ROSAT all-sky survey [15] and is estimated to be at a distance of 1 kpc [16]. The source is consistent with a core-collapse SNR (type II), for which the stellar winds from the high-mass progenitor evacuated the surrounding matter prior to the SN explosion [17], which is also suggested by observations [18]. Correlation studies between the interstellar gas, X-ray and γ -ray emissions provide evidence for hadronic γ -ray emission in addition to the broadband emission spectra [19]. These results are in agreement with the hadronic component observed in the MWL analysis of [9]. Furthermore, simulations reveal that with an exposure time of 50 hours, CTAO would be able to identify the dominant γ -ray emission component from the morphology study of the SNR [20].

2.2.2 HAWC J2227+610

HAWC J2227+610 (also called SNR G106.3+02.7) was first discovered by the Northern Galactic Plane survey with the Dominion Radio Astrophysical Observatory (DRAO; [21]) and is located at a distance of 800 pc [22]. To the North of the head region, there is a pulsar wind nebula (PWN) called "Boomerang". It is powered by the pulsar PSR J2229+6114 (associated with LHAASO J2226+6057, [23]) formed from the core-collapse SN explosion leading to the SNR G106.3+2.7 [24]. The VERITAS collaboration detected significant TeV γ -ray emission from the elongated radio extension of this SNR [25]. The extended γ -ray emission spatially coincides with molecular clouds traced by ^{12}CO (J = 1 - 0) emission [22, 26], favouring a hadronic origin of the γ -ray emission, also supported by [9]. However, the origin of the emission remains unclear, with three possible sources: hadronic, leptonic, or a combined process. According to [27], CTAO would provide information on the morphology of the source, with a significant detection of the extension of the source, thereby providing clearer evidence on the origins of the γ -ray emission.

The global parameters of RX J1713.7-3946 and HAWC J2227+610 are detailed in Table 1.

Table 1: The characteristics of the studied SNRs, together with the references for the data. Shell: most of the radiation comes from a shell of shocked material. Int.: SNR is interacting with the surrounding medium.

Sources	RX J1713.7-3946	HAWC J2227+610
Type	Shell	Int.
Distance (kpc)	1	0.8
Galactic coordinates (deg)	(347.34,-0.47)	(106.58,2.91)
High-energy γ -ray data	ASDC/Suzaku[28]/ <i>Fermi</i> [29]/H.E.S.S [30]	ASDC/Chandra/ <i>Fermi</i> - <i>LAT</i> [31], VERITAS[25], LHAASO[23] and HAWC[32]

3 Evolution of the particle spectrum

3.1 Composition of the CRs

As discussed in Section 1, the SNRs are believed to accelerate CRs up to the "knee" energies due to their large energy budget. In the simple Hillas formalism, the maximum energy for CRs obtained in the acceleration mechanism is proportional to the charge of the nucleus [33]. Therefore, heavier nuclei with charge Z get accelerated to energies Z times larger. This seems to be confirmed by the fact that the chemical composition at the knee shows a transition from light to heavier nuclei, from the "proton knee" at 3 PeV to the "iron knee" at about 90 PeV. In the following, we discuss several predictions and measurements of the CR composition at various energies. These compositions are shown in Figure 1.

The composition of CRs measured at around 1 GeV is mainly protons (89%), including helium nuclei (10%) and heavier nuclei (1%) [34]. The CR composition measured by the Alpha Magnetic Spectrometer (AMS) detector at 1 TeV [35] (*1 TeV SN from AMS*, Figure 1) and measured at around 1 GeV [36] (*0.07-0.28 GeV/A CRs*, Figure 1) was found to be characterized by a general overabundance of light elements such as protons and He. [37] also used this GCR composition at around 1 GeV to consider the amount of energy channelled into CRs by a single SN event (*Energy injected/SN*, Figure 1).

With increasing energy, the proportion of heavy nuclei becomes important (*1 PeV GW-CRs* in Figure 1) for a CR composition at 1 PeV. This energy would be available if we consider the re-acceleration of the CRs by the Galactic wind termination shock of the SNR [37].

On the other hand, the composition is related to the type of the source. In the case of a core-collapse SN (Type II) such as RX J1713.7-3946 or HAWC J2227+610, an important contribution of heavy elements, including CNO, Ne, Mg, Si and Fe, is observed [38] (*Type II SN from chemical evolution model* in Figure 1). Primary CRs (He, CNO, Ne, Mg, Si, Fe,...) are synthesised in stars and accelerated by astrophysical sources. The Fe nuclei are thought to be synthesized mainly in core-collapse SNs of massive stars. Its radioactive lifetime of 3.8 Myr is sufficiently long, so that it can potentially survive the time interval between the nucleosynthesis and the detection at Earth [39].

Finally, even at low energies (around 1 GeV), the CR composition can exhibit a general overabundance of heavy elements relative to protons and helium due to the interaction of CRs with the gas and dust environment [40] (*0.1-1 GeV/A sources-environment-CRs* in Figure 1).

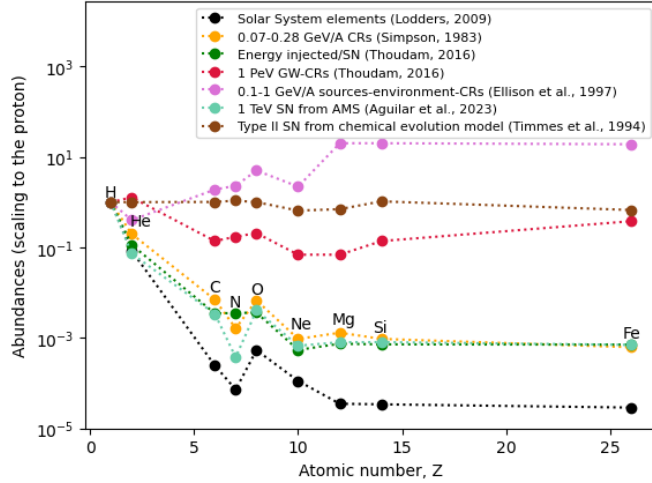


Figure 1: Different CR compositions. See text.

In Figure 1, one can also see the elemental composition of the Solar System [41] (*Solar System elements*), which is different from the CR composition due to the propagation effects of CRs.

The two SNRs considered in this study are both core-collapse SNRs. Therefore, we have considered the composition of type II SN. In addition, we have considered GCR composition measured at 1 PeV. These two CR compositions are indicated by the brown and red points in Figure 1.

3.2 Acceleration models

The differential energy distribution of accelerated hadrons, $n(E)$, is in the following assumed to follow a simple power-law with spectral index α and an exponential cutoff at an energy E_{cutoff} , with sharpness described by the parameter β : $n(E) \propto E^{-\alpha} e^{-(\frac{E}{E_{\text{cutoff}}})^\beta}$.

Studying the shape of the energy spectra of CR particles gives us information on the underlying acceleration mechanisms. Various physical processes, such as absorption by the source or interactions with its surrounding environment, can potentially influence this particle spectrum shape. According to [42], the CRs accelerated at the SNR, which originated from a massive star in a molecular cloud, diffusively penetrate the dense clumps that survive inside the SNR. This implies that the spectrum of the CRs inside the clumps may well be significantly harder than the one accelerated at the shock [43, 44].

According to [45], the exact shape of the cut-off in the spectrum depends, in principle, on what is limiting the acceleration. Assuming that the main mechanism responsible for CR acceleration is DSA [5], the most stringent constraint is usually imposed by the size of the accelerator compared to the diffusion distance of the highest energy particles. The diffusion coefficient D can be expressed as $D(E) = D_0 E^\beta$, where D_0 is a normalisation coefficient and β is related to the sharpness of the cutoff (β in Eq. 4.2.1). In particular, an exponential cut-off is found for Bohm diffusion ($\beta = 1$), while sub-exponential cut-offs result from other diffusion models commonly used in astrophysics, such as Kolmogorov's ($\beta = 1/3$) or Kraichnan's ($\beta = 1/2$) models. It is expected that SNRs can reach energies close to the "knee" energy only by considering the so-called non-resonant streaming instability [46], which is induced by the particles at the instantaneous maximum energy leaving the

accelerator. In this scenario, the spectrum at the shock is usually assumed to be cut very sharply at E_{\max} , which would reflect the case of super-exponential cut-offs ($\beta > 1$).

Regarding RX J1713.7-3946, it is expected that the origin of the γ -ray emission would be hadronic if the SNR expands in a clumpy medium [47, 48]. The presence of clumps can explain the observed γ -ray spectrum of RX J1713.7-3946, which is generally considered too hard to be explained by hadronic interactions. According to simulations, the interaction between the SNR and the clumps would lead to a strong amplification of the turbulent magnetic field at the interface between the clumps and the diffuse gas. High-energy CRs would penetrate the clumps, exhibiting a faster diffusion. Consequently, the CR spectrum within the clumps is expected to be considerably harder than that of CRs in the SNR shell [49].

These arguments led us to consider proton acceleration models with different diffusion scenarios with $\beta = 0.5$ to $\beta = 1.5$.

4 Modelling and simulation of the γ -ray spectra for CTAO

4.1 Modelling with GAMMAPY

The modelling of the γ -ray spectra were exclusively conducted using the GAMMAPY package [50]. GAMMAPY is an open-source analysis package developed to facilitate high-level analysis of IACT data. It includes tools to perform Markov Chain Monte Carlo (MCMC) fitting of radiative models to X-ray and γ -ray spectra using *emcee*, an affine-invariant ensemble sampler for MCMC [51]. We used the NAIMA package [52] to build our models based on the non-thermal radiation from relativistic particle populations. For more details, see Section 4.3.1.

4.2 γ -ray spectrum modelling

4.2.1 Particle spectrum by SNR

For a strong shock, such as in the case of SNRs, the particle prediction from shock acceleration theory gives a universal power law spectrum of accelerated particles, expressed as $Q_{\text{CR}}(E) \propto E^{-\alpha}$, where the spectral index α is typically set to 2 [6].

The particle energy distribution function or particle function or particle distribution $n(E)$ is expected to follow an exponential cut-off power-law (EPL), expressed as:

$$n(E) = A_m \left(\frac{E}{E_0} \right)^{-\alpha} e^{-\left(\frac{E}{E_{\text{cutoff}}}\right)^\beta} \quad (4.1)$$

with:

- A_m : amplitude of the proton distribution (A_m^p) or electron distribution (A_m^e)
- E_0 : reference energy typically set to 1 TeV
- α : proton spectral index (α_p) or electron spectral index (α_e)
- E_{cutoff} : proton cut-off energy (E_{cutoff}^p) or electron cut-off energy (E_{cutoff}^e)
- β : cut-off exponent/sharpness

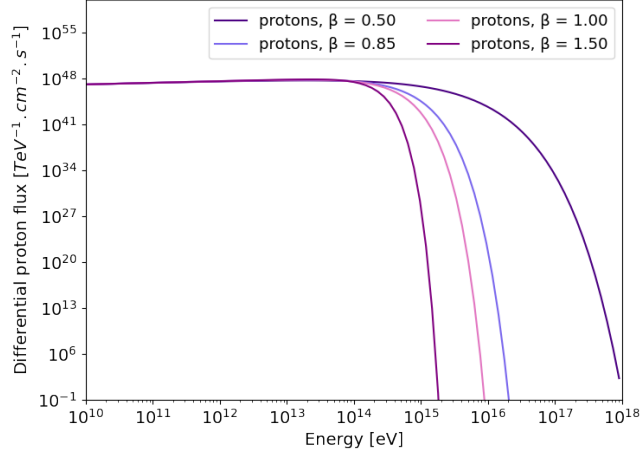


Figure 2: Proton distributions for $\beta = 0.50, 1.00, 0.85,$ and 1.50 .

The proton particle function is given by: $n_p(E) = A_m^p \left(\frac{E}{E_0}\right)^{-\alpha_p} e^{-\left(\frac{E}{E_{\text{cutoff}}^p}\right)^\beta}$.

If we consider heavier nuclei, $n_p(E)$ can be modified following the approach proposed by [37]. This modification incorporates f , the fraction of the abundance of the considered CRs, and an increased proton energy $Z \times E_{\text{cutoff}}^p$ where Z is the charge of the CR. The modified function is expressed as:

$$n_p^Z(E) = f A_m^p \left(\frac{E}{E_0}\right)^{-\alpha_p} e^{-\left(\frac{E}{Z \times E_{\text{cutoff}}^p}\right)^\beta} \quad (4.2)$$

For the fraction of the abundance f , we have taken the composition at 1 PeV and the composition of the type II SN, as discussed before (see Section 3.1).

Considering different acceleration models as mentioned in Section 3.2, different sharpnesses were studied. A range of values from $\beta = 0.50$ to $\beta = 1.50$ was considered and this study was performed only for protons for RX J1713.7-3946. Figure 2 illustrates the proton spectrum for $\beta = 0.50, \beta = 0.85, \beta = 1.00$ and $\beta = 1.50$. The spectral parameters of the proton distribution are fixed by the MWL study of RX J1713.7-3946 [9].

4.2.2 γ -ray spectrum from the π^0 decay process

In the following, we have considered only hadronic models. As discussed before, in the case of the two studied SNRs, the hadronic component was the most important one at the highest energies. In section 5.4, we compare the results obtained by using both, hadronic and leptonic (IC) models.

The inelastic collisions producing π^0 are based on Glauber's multiple scattering theory [53] that takes into account the inelastic interaction cross-section for protons [54] and for heavier nuclei [55]. The cross-section, σ , depends on the mass numbers of the projectile and the target, A_{pro} and A_{tar} , the projectile and target mass number, respectively, as well as on the kinetic energy of the projectile, T_{pro} . The cross-section, σ , relies on experimental data (π_0 spectra), simulations from *Geant4* (interaction between particles with and surrounding matter), and hadronic models.

(a) Proton distribution.		
	RX J1713.7-3946	HAWC J2227+610
A_m^p [TeV ⁻¹]	$(1.15 \pm 1.00) \times 10^{47}$	$(1.05 \pm 1.00) \times 10^{47}$
α^p	1.75 ± 0.02	1.76 ± 0.03
E_{cutoff}^p [TeV]	77.75 ± 1.10	444.16 ± 1.17
N_H [cm ⁻³]	21.03 ± 1.05	1.70 ± 0.10
K_{ep} [cm ⁻³]	0.0139 ± 0.0006	0.00476 ± 0.00004
(b) Electron distribution.		
	RX J1713.7-3946	HAWC J2227+610
A_m^e [TeV ⁻¹]	$(3.16 \pm 1.04) \times 10^{46}$	$(2.69 \pm 1.08) \times 10^{45}$
α^e	2.47 ± 0.04	1.69 ± 0.03
E_{cutoff}^e [TeV]	23.15 ± 1.07	0.69 ± 1.00
N_H [cm ⁻³]	21.03 ± 1.05	1.70 ± 0.10
K_{ep} [cm ⁻³]	0.0139 ± 0.0006	0.00476 ± 0.00004

Table 2: Parameters obtained from the lepto-hadronic fit of the γ -ray spectrum of RX J1713.7-3946 and HAWC J2227+610 for proton and electron distributions (from [9]). NB: K_{ep} represents the ratio of electrons with respect to protons at 1 TeV.

The photon flux $F_p^Z(E)$, is given by this equation:

$$\begin{aligned}
 F_p^Z(E) &= f\sigma N_H A_m^p \left(\frac{E}{E_0}\right)^{-\alpha_p} e^{-\left(\frac{E}{Z \times E_{\text{cutoff}}^p/A}\right)^\beta} \\
 &= f\sigma N_H A_m^p \left(\frac{E}{E_0}\right)^{-\alpha_p} e^{-\left(\frac{E}{E_c^Z}\right)^\beta}
 \end{aligned} \tag{4.3}$$

with σ , the inelastic cross-section between GCRs and stationary protons, N_H , the number density of the target protons and A , the mass number of the nuclei of the considered GCRs.

Note that the cutoff energy in the photon spectrum for heavy CRs ($E_c^Z = Z \times E_{\text{cutoff}}^p/A$) is lower than that for protons (E_{cutoff}^p). This is due to the fact that for the π^0 creation, the relevant energy is the energy per nucleon. Thus, we expect a softening of the γ -ray spectrum in case of heavy CRs.

We used the radiative PD-model from NAIMA by fixing the parameters of the proton distribution A_m^p , E_0 , α^p , E_{cutoff}^p , β as well as the number density of the target protons N_H (the density at rest is similar for protons and heavier nuclei) according to the MWL study [9]. The fixed MWL parameters are reported in the Table 2.

We computed, with the NAIMA spectral model class, the non-thermal emission from populations of relativistic GCRs due to interactions with the surrounding matter by fixing the distance of the source under consideration (see Table 1). **In case of composed models, such as p+CNO or p+Fe, we have combined the different individual models by using the GAMMAPY compound spectral model class.**

The γ -ray spectra resulting from the radiative PD-models by using the particle distributions of protons and heavier nuclei (He, C, N, O, Ne, Mg, Si, Fe, p+CNO) with 1 PeV GCRs and a type II SN composition, are shown in Figure 3. One can observe that the different particle distributions yield different photon distributions. Therefore, one can expect that by measuring the photon distribution

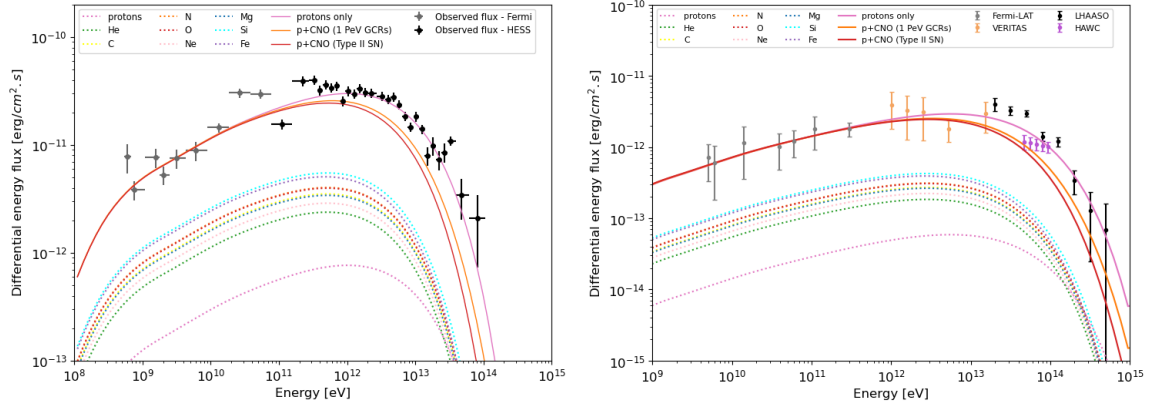


Figure 3: γ -ray spectra considering PD-models for different nuclei considering a type II SN composition (individual nuclei in dotted lines) and protons-only and composed PD-models (solid lines). Left: RX J1713.7-3946. Points correspond to measured data from *Fermi* [29] and H.E.S.S. [30]. Right: HAWC J2227+610. Points correspond to measured data from *Fermi-LAT* [31], VERITAS [25], LHAASO [23] and HAWC [32]. See text.

with high accuracy, the underlying particle distribution can be deduced, thereby throwing light on the nature of CRs.

Note also that due to the global normalization, in case of 'p+CNO', the proton flux is lower than in case of 'protons only' (depending on the chosen composition, either '1 PeV GCRs' or 'type II SN').

4.3 CTAO γ -ray spectrum simulation

4.3.1 Simulating with GAMMAPY

The simulations were performed by using the **most recent version of** GAMMAPY package [56] and the Cherenkov Telescope Array Observatory Instrument Response Functions (CTAO IRFs) available online (see Section 6 - Data Availability). The CTAO IRFs are determined by Monte Carlo simulations and based on the mapping between the incoming photon flux and the detected events of the γ -ray shower. GAMMAPY provides functionalities to reduce simulated events by binning them in energy and sky coordinates defined by a single region on the sky. Several techniques for the background estimation are implemented in the package. The counts data and the counts after the background subtraction are bundled into datasets. Additionally, **the GAMMAPY Maker class** provides the simulated data points using radiative models through the NAIMA package [52] (**NAIMA spectral model class**). **The spectral parameters are input parameters of the radiative models.** The data can be regrouped to compute flux points in a specific energy band **with the GAMMAPY Estimators class**. The flux of γ -ray sources can be estimated using Poisson maximum likelihood fitting.

We have simulated the CTAO spectrum with a 1D On-Off analysis. This consists of measuring the spectrum of the source in a given region defined on the sky with a circular aperture centered on the region of interest ("ON-region") with a specific energy binning. To estimate the expected background in the "on region", fake off-counts are simulated with a Poisson fluctuation considering the acceptance, which is the relative background efficiency in the "OFF-region". The data were modelled using IC and/or π^0 decay models. Based on the best-fit model, the final flux points and corresponding

log-likelihood profiles were computed.

These simulations were performed on extended sources, as it is the case for RX J1713.7-3946 and HAWC J2227+610. The 1D analysis approach was chosen because RX J1713.7-3946 and HAWC J2227+610 are isolated sources. Using gamma-sky.net, we can see that the other γ -ray sources in the region do not overlap with these sources. If there are overlapping sources or complex morphology, a 3D analysis would be necessary.

4.3.2 Input parameters for simulations

For the simulations with `GAMMAPY`, we have used IRFs *prod5 version v0.1* (see Section 6 - Data Availability) to get the predicted number of counts. IRFs are provided for both sites (Southern or Northern), for 3 different zenith angles of the source (20° , 40° or 60°) and for 3 different observation times (0.5 h, 5 h or 50 h).

To run simulations, we defined the following observational parameters:

- Zenith angle: the visibility plot on the *TeVCat* database [57] allowed us to choose the optimal zenith angle for observing the sources.
- Livetime: we set the observation time to 50 h (or 200 h). To be more realistic, we divided this lifetime into 67 (or 267) observation runs of 45 min each, which we stacked.
- Offset: we set the offset to 1° . This results in a radii greater than the radii of the source, ensuring coverage of the entire source area.
- ON-region: this corresponds to the radii of the sources, 0.65° and 0.23° for RX J1713.7-3946 and HAWC J2227+610, respectively.
- Energy range: the flux was simulated in the energy range from 3×10^{10} eV to 1.99×10^{14} eV.
- Exclusion region: susceptible γ -ray sources can be localised close to the studied source. They have been determined through gamma-sky.net. These sources do not overlap the studied sources, as explained previously.

The following particle distributions and radiative models were used to simulate the γ -ray spectrum for RX J1713.7-3946 and HAWC J2227+610:

- A composed model of protons and heavier nuclei (protons + CNO, protons + Fe) together with the radiative PD-model.
- A model of protons with different sharpnesses ($\beta=0.50, 0.85, 0.90, 0.95, 1.00, 1.05, 1.10, 1.15, 1.50$) together with the radiative PD-model.
- A composed model of protons and heavier nuclei (protons + CNO) with the radiative PD-model and electrons with the IC radiative model (PD(p+CNO) + IC(e^-)).

The simulations were performed by using IC and π^0 -decay radiative models with the parameters obtained from the MWL study (see Table 2).

In the case of HAWC J2227+610, the optimal zenith angle is 60° . The air attenuation is significant for high zenith angles; therefore, we decided to simulate the data at 40° . The area for collecting photons at

Table 3: Input parameters for CTAO simulations for RX J1713.7-3946 and HAWC J2227+610.

	RX J1713.7-3946	HAWC J2227+610
Zenith angle [deg]	20	40
Lifetime [h]	50	50
Offset [deg]	1	1
Site location	South: 14 MSTs / 37 SSTs	South: 14 MSTs / 37 SSTs
ON region radii [deg]	0.65	0.23
Energy range [TeV]	$[30 \times 10^{-3}, 199]$, bin=31	$[30 \times 10^{-3}, 199]$, bin=31
Exclusion region	CTB 37A (SNR G348.5+0.1)	SNR G106.6+2.9
Tested models	PD: protons/p+CNO/p+Fe/p($\beta \neq 1$)	PD: protons/p+CNO/p+Fe
	PD+IC: p+CNO+ e^-	PD+IC: p+CNO+ e^-
Extended source	Yes	Yes

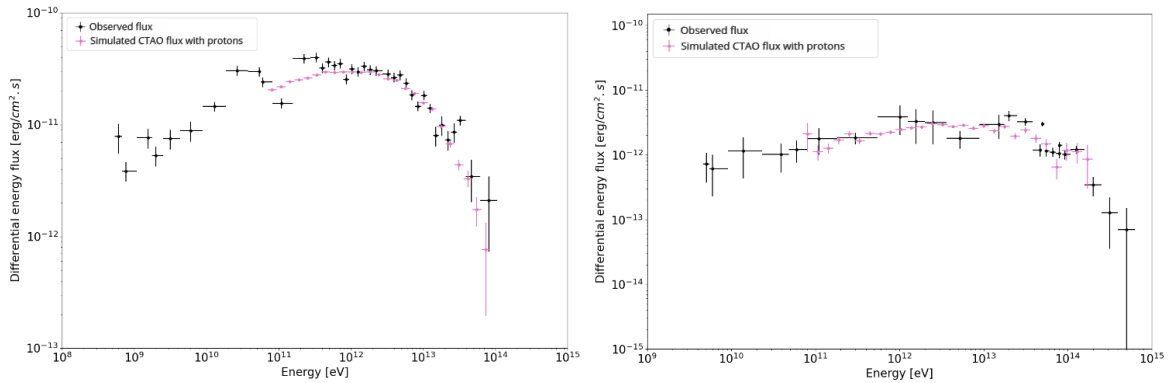


Figure 4: Left: CTAO simulation for the γ -ray spectrum of RX J1713.7-3946 using proton distribution (pink points). Black points correspond to measured data from *Fermi* [29] and H.E.S.S [30]. Right: CTAO simulation for the γ -ray spectrum of HAWC J2227+610 using proton distribution (pink points). Black points correspond to measured data from *Fermi-LAT* [31], VERITAS [25], LHAASO [23] and HAWC [32]. See text.

40° is smaller than that at 60° , resulting in lower statistics but more data points at the highest energies. In the case of RX J1713.7-3946, the optimal zenith angle is 20° , which was used for simulations. The different input parameters are indicated in Table 3.

In Figure 4, we compare the CTAO simulations to currently existing observations. For the simulations, we supposed a proton distribution and a radiative PD-model shown in Figure 3. The data points simulated at the limits of the energy range were not considered because of the instrumental uncertainty. As can be seen, we observe an accurate reconstruction of the CTAO flux and a good agreement with the currently existing data. However, it is important to note that each instrument has a different level of systematic uncertainty. In the following, these existing data points have not been included in the fit procedure.

4.3.3 Data fitting and likelihood test

The quality of the simulation was assessed by using the *Minuit* optimizer [58], which is accessible through `GAMMAPY`'s `FIT CLASS`. The simulated fluxes were fitted using different models to determine how closely they matched the input model. A lower Loglikelihood value indicates a smaller difference between the simulated flux and the models.

The log-likelihood test (TS) was realized with the maximum log-likelihood ratio λ given by $\lambda = \mathcal{L}_1/\mathcal{L}_0$ with 0 and 1 corresponding to the two models that are compared. The ΔTS value is given by: $\Delta TS = TS_1 - TS_0 = -2\ln(\lambda)$ where TS_0 and TS_1 are given by the statistics of the fit (`total_stat`) using a *Minuit* minimizer (returning `-2LogLike`). This statistic behaves like a chi-squared function, i.e. the minimum of the function in repeated identical random trials is chi-squared distributed up to an arbitrary additive constant. Hence, ΔTS follows the χ^2 distribution with n_{dof} degrees of freedom, i.e. the difference in the number of free parameters between the models (0 and 1).

We assumed that a significance larger than 5σ indicates that the two models can be distinguished. This significance corresponds to ΔTS equal to 25 for 1 degree of freedom and 29 for 2 degrees of freedom.

5 Results

5.1 CTAO sensitivity to heavy nuclei

This study aims to determine whether CTAO can detect heavy GCRs. To achieve this, we simulated the CTAO flux for RX J1713.7-3946 and HAWC J2227+610 using a radiative PD-model with protons-only distribution and a composed distribution of protons + CNO and protons + Fe (see Section 4.3.2). The simulations were performed for 1 PeV GCRs and type II SN compositions. The fits were performed by using the radiative PD-model with the following free parameters for each source (see Section 4.2.1):

- RX J1713.7-3946: amplitude A_m^P , spectral index α^P .
- HAWC J2227+610: amplitude A_m^P .

In the case of HAWC J2227+610, the flux is approximately 150 times lower than that of RX J1713.7-3946, and the use of only 1 free parameter allowed the fit to converge. The other model parameters were taken from the MWL study, see Table 2. The results are shown in Figure 5.

Table 4a presents the statistical results of the likelihood tests ΔTS , obtained when comparing the two models. We assume that a ΔTS value greater than 25 (only 1 free parameter) or 29 (2 free parameters) indicates that CTAO can distinguish the two models. One can see that high values ($\gg 29$) were obtained for RX J1713.7-3946 in the case of using 2 free parameters. As an example, Table 4b shows the parameters obtained from the fit of RX J1713.7-3946. These results indicate that CTAO would be capable of distinguishing between protons-only and p+CNO or p+Fe considering the two different GCRs compositions (1 PeV GCRs and type II SN).

Similar conclusions are obtained for HAWC J2227+610 with slightly lower statistical significance and by using only one free parameter.

(a) Log-likelihood tests comparing γ -ray spectra given by heavy CRs distribution (p + CNO, p + Fe) with proton distribution. Two compositions for heavy CRs are used: 1 PeV GCRs and type II SN.

	RX J1713.7-3946	HAWC J2227+610
TS[p+CNO (1 PeV GCRs)] - TS[p]	102	53
TS[p+CNO (Type II SN)] - TS[p]	202	113
TS[p+Fe (Type II SN)] - TS[p]	188	88

(b) Example of the parameters obtained from the fit of RX J1713.7-3946. A_m^p and α^p are set free during the fit.

	p+CNO (1 PeV GCRs)	p+CNO (Type II SN)	p+Fe (Type II SN)
A_m^p [TeV ⁻¹]	$(7.62 \pm 1.13) \times 10^{46}$	$(7.91 \pm 1.20) \times 10^{46}$	$(2.17 \pm 0.14) \times 10^{47}$
E_0 [TeV]	1.00	1.00	1.00
α^p	(1.75 ± 0.06)	(1.77 ± 0.06)	(1.76 ± 0.02)
E_c^Z [TeV]	38.88	38.88	36.10
β	1.00	1.00	1.00

Table 4: Fit results.

5.2 CTAO sensitivity to different proton acceleration models

The flux of RX J1713.7-3946 was simulated for CTAO using the PD-model for three different proton distributions with $\beta = 0.50, 1.50$ and 0.85 (see Section 4.2.1). The results of the simulation are compared to measured data in Figure 6 (left). One can observe a good agreement between measured data and simulations with $\beta = 0.85$. It is again noted that Figure 7 allows us only qualitative comparison; in the following, the fit procedure is performed only for simulated CTAO data.

Figure 6 (right) shows the results of the simulation with $\beta = 0.85$ together with the fit results for $\beta = 0.85$ and $\beta = 1.00$. This leads to a difference between the log-likelihood tests $\Delta TS = 32$ using 2 free parameters (A_m^p and α^p), showing that CTAO would be able to distinguish between these two β values.

In order to determine the CTAO sensitivity to distinguish between different β values, we simulated CTAO data by using several β values around 1.00, from 0.85 to 1.15, with a step of 0.05. These simulations were performed for an observation time of 50 h and 200 h. As an example, Figure 7 shows the comparison of $\beta=0.90$ and $\beta=1.00$. This leads to a difference between the log-likelihood tests $\Delta TS = 9$ for 50 h and $\Delta TS = 46$ for 200 h. These results indicate that 50 h would not be sufficient to distinguish a β variation of 0.10. Longer observation time increases statistics, resulting in better sensitivity for different β values. Table 5 shows a compilation of all results obtained for different β values using 50 h and 200 h observation times. The statistical analysis is performed by comparing simulations with different β values to the model of $\beta=1.00$. One can observe that for 200 h, a β variation as small as 0.10 can be distinguished. In the case of 50 h, only variations larger than 0.15 can be differentiated.

This study shows that CTAO is sensitive to the shape of the particle distribution and, therefore, could provide information on different acceleration models.

5.3 CTAO sensitivity to separate heavy nuclei and proton acceleration models

The goal of this study was to determine whether CTAO could differentiate between the contribution of heavy nuclei and different β values. This was done by simulating CTAO fluxes for an observation time of 50 h using a proton distribution with $\beta=0.85$ and a protons+CNO distribution with $\beta=1.00$.

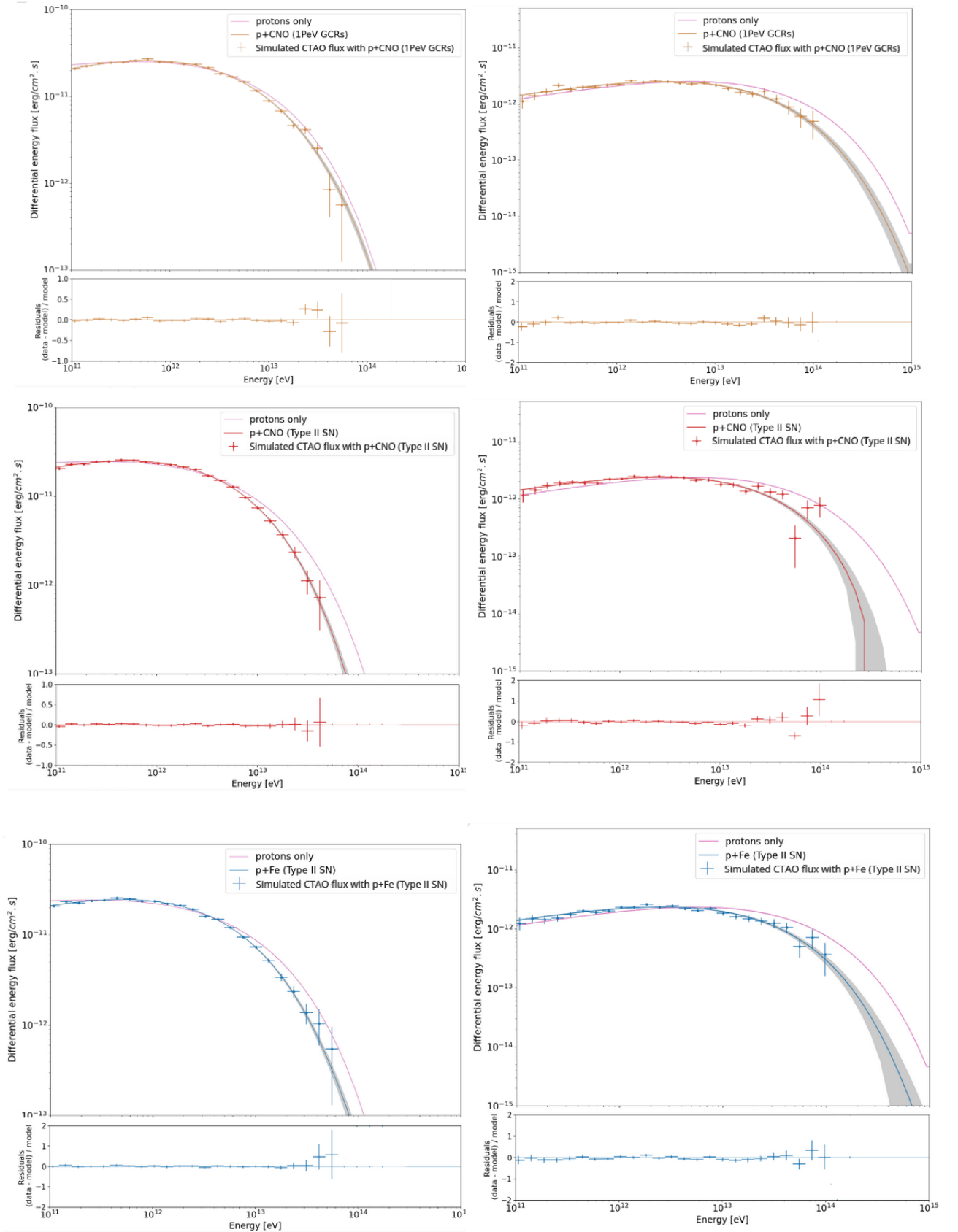


Figure 5: Left: CTAO simulations for the γ -ray spectrum of RX J1713.7-3946 (points) with models indicated in the figure. Right: CTAO simulations for the γ -ray spectrum of HAWC J2227+610 (points) with models indicated in the figure. The results of the fit with different models are shown in solid lines. The shaded area shows the uncertainties of the fit.

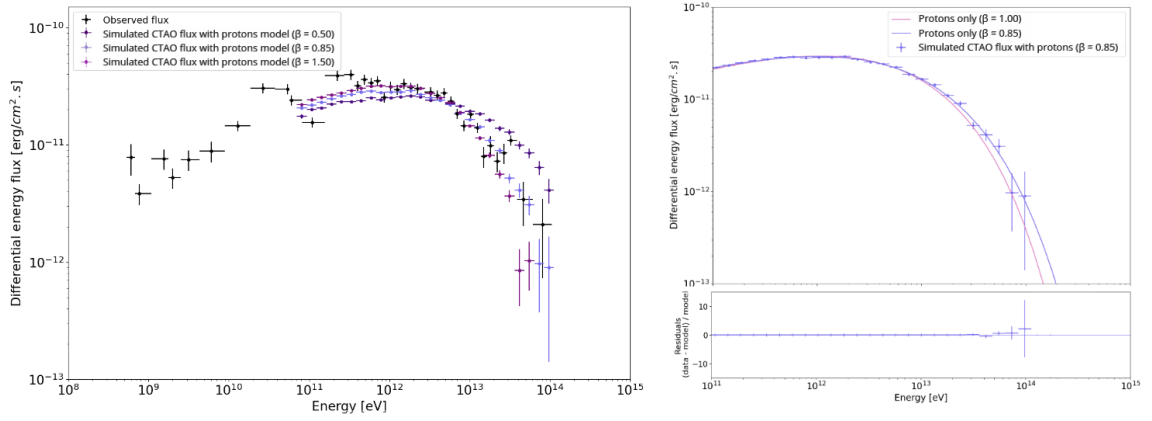


Figure 6: Left: CTAO simulations for the γ -ray spectrum of RX J1713.7-3946 by using different β values for proton distribution (see figure insert). Black points correspond to measured data from *Fermi* [29] and H.E.S.S [30]. Right: CTAO simulation for the γ -ray spectrum by using proton distribution with $\beta = 0.85$ (purple points). Fit results for proton models considering $\beta = 1.00$ (pink solid line) and $\beta = 0.85$ (purple solid line).

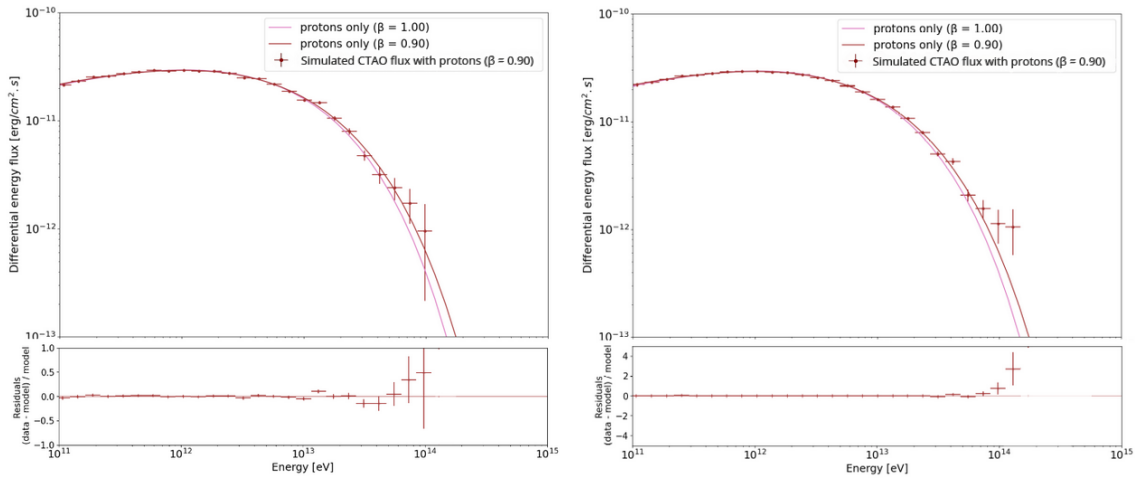


Figure 7: CTAO simulation for the γ -ray spectrum of RX J1713.7-3946 by using proton distribution with $\beta = 0.90$ (brown points). Fit results for proton models considering $\beta = 1.00$ (pink solid line) and $\beta = 0.90$ (brown solid line). Left: results for 50 h of observations. Right: results for 200 h of observations.

Table 5: Log-likelihood tests comparing CTAO simulations for the γ -ray spectrum of RX J1713.7-3946 by using proton distribution with different β values to that with $\beta=1.00$.

		β	0.50	0.85	0.90	0.95	1.05	1.10	1.15	1.50
50 h	TS[p(β)] - TS[p($\beta = 1$)]		649	33	7	2	7	4	7	98
200 h	TS[p(β)] - TS[p($\beta = 1$)]		2500	98	48	11	4	23	40	471

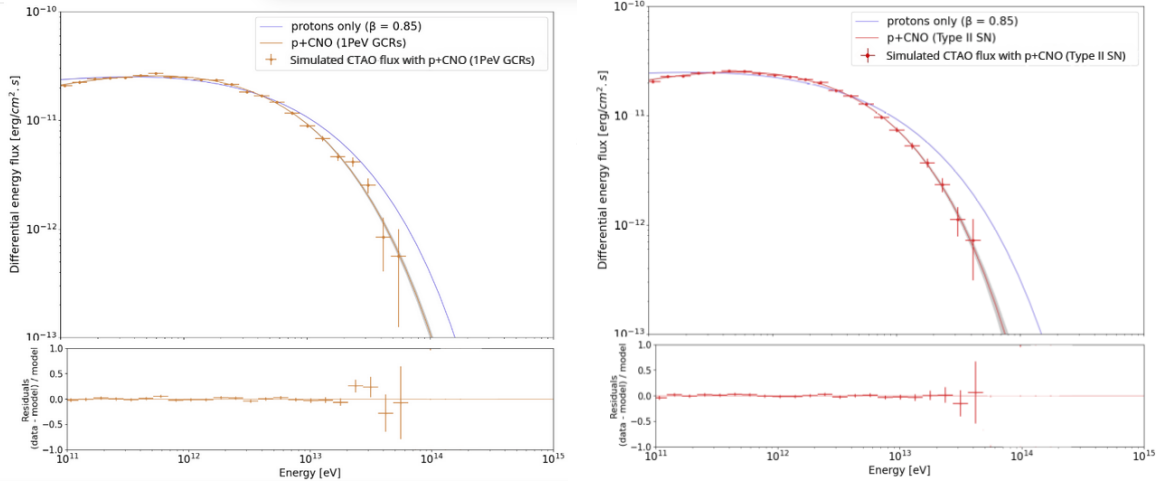


Figure 8: Left: CTAO simulation for the γ -ray spectrum of RX J1713.7-3946 by using a p+CNO distribution with a 1 PeV composition (orange points). Fit results for a proton distribution with $\beta=0.85$ (blue solid line). Right: CTAO simulation for the γ -ray spectrum of RX J1713.7-3946 by using p+CNO distribution with a type II SN composition (red points). Fit results for a proton distribution with $\beta=0.85$ (blue solid line).

Table 6: Log-likelihood tests comparing γ -ray spectra given by heavy CRs distribution (p + CNO) with proton distribution ($\beta=0.85$) for RX J1713.7-3946. Two compositions for heavy CRs are used: 1 PeV GCRs and type II SN.

Composition for p+CNO	1 PeV GCRs	Type II SN
TS[p+CNO] - TS[p ($\beta = 0.85$)]	191	317

For the CR composition, type II SN and 1 PeV GCRs were used.

The results are shown in Figure 8. Table 6 compiles all obtained results. As can be seen, Δ TS values for all combinations are greater than 29, indicating that CTAO can distinguish between different CR compositions and β values. This is due to the shape of the γ -ray spectrum, which is different for heavy nuclei compared to the proton spectrum with different β values. Therefore, we can conclude that the high resolution and the sensitivity of CTAO would allow us to distinguish between the contribution of heavy nuclei and different β values. However, to do such studies, it is necessary to perform MWL analysis [9] in order to fix some of the spectral parameters.

We also studied the use of **NAIMA Exponential Cutoff Broken Power Law (EBPL) distribution instead of EPL for CRs**. The results show that there is no significant change in the conclusions. This can be understood since the shape of the spectrum induced by adding heavy nuclei is clearly different from other types of cutoff shapes (different β values or using different distributions, EPL or EBPL).

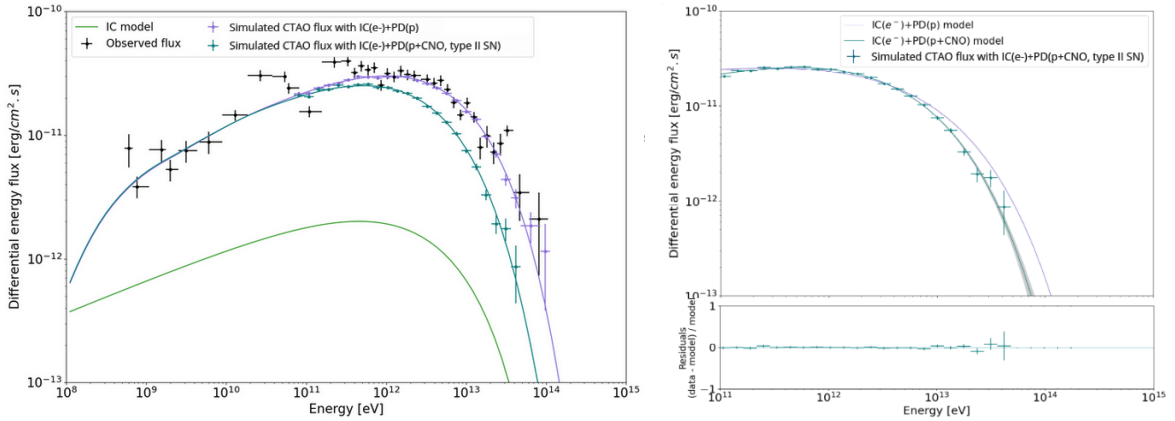


Figure 9: Left: CTAO simulations for the γ -ray spectrum of RX J1713.7-3946 by using PD+IC-model with proton distribution (purple points) and PD(p+CNO)+IC-model with p+CNO distribution (blue points, see figure insert). The solid green line corresponds to the IC contribution. Black points correspond to measured data from *Fermi* [29] and H.E.S.S. [30]. Right: CTAO simulation for the γ -ray spectrum by using PD(p+CNO)+IC-model considering a type II SN composition (blue points). Fit results for the PD+IC-model (purple solid line) and for the PD(p+CNO)+IC-model (blue solid line).

Table 7: Log-likelihood tests comparing γ -ray spectra given by heavy CRs and electron distributions ($p + \text{CNO} + e^-$) with proton and electron distributions ($p + e^-$). The type II SN composition for heavy CRs was used.

Source	RX J1713.7-3946	HAWC J2227+610
TS[$p+\text{CNO}+e^-$] - TS[$p+e^-$]	180	105

5.4 Contribution of electrons

Up to now, we have considered only hadronic scenarios with the PD-model. As discussed before, hadronic contribution dominates at the highest energies in the case of the two studied sources. Finally, to study the possible impact of electrons on the previous conclusions, we have included electron distribution and the IC radiative model by using the parameters from the MWL study (see Table 2). The parameters for the electron distributions are mostly fixed by the synchrotron and bremsstrahlung contributions at low energies.

We have simulated CTAO flux by using a composed model of PD(p+CNO)+IC and fitted it with a composed model of PD(p)+IC. A composition of a type II SN for p+CNO nuclei was used and $\beta=1.00$ was taken for both models. The parameters A_m^p and α^p for PD-models were kept free during the fit for RX J1713.7-3946. For the fit for HAWC J2227+610, only A_m^p for PD-models was kept free. The results are shown in Figure 9 for RX J1713.7-3946 and in Figure 10 for HAWC J2227+610. The ΔTS test gave high values: 180 for RX J1713.7-3946 and 105 for HAWC J2227+610 (see Table 7). These results show that the inclusion of electron distribution and IC model still **allow** us to distinguish between protons and p+CNO. This is consistent with the analysis realized in Section 5.1 by using only hadronic models. However, a MWL analysis is necessary to fix the parameters of the IC-model.

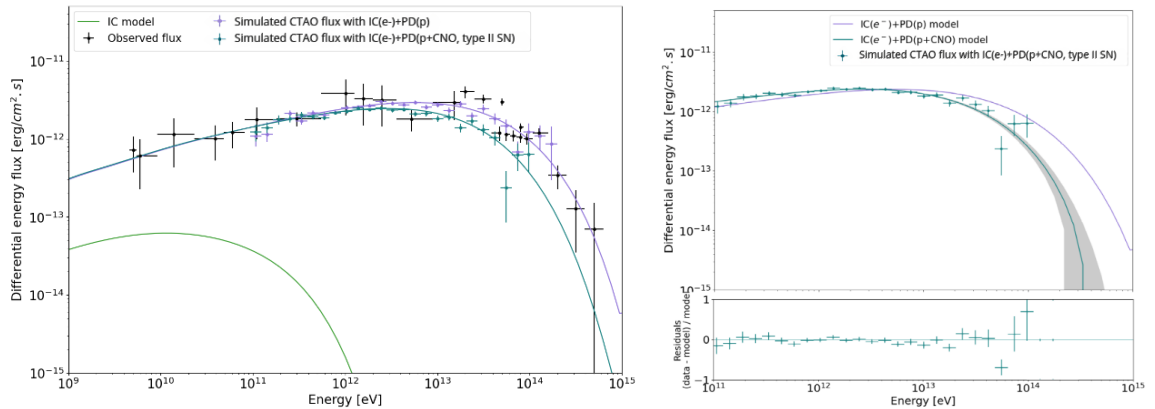


Figure 10: Left: CTAO simulations for the γ -ray spectrum of HAWC J2227+610 by using a PD+IC-model with proton distribution (purple points) and PD(p+CNO)+IC with p+CNO distribution (blue points, see figure insert). The solid green line corresponds to the IC contribution. Black points correspond to measured data from *Fermi-LAT* [31], VERITAS [25], LHAASO [23] and HAWC [32]. Right: CTAO simulation for the γ -ray spectrum by using PD(p+CNO)+IC-model considering a type II SN composition (blue points). Fit results for the PD+IC-model (purple solid line) and for the PD(p+CNO)+IC-model (blue solid line).

6 Conclusions

We have studied the impact of CTAO on the spectral shape sensitivity in the cases of two SNRs: RX J1713.7-3946 and HAWC J2227+610. These SNRs were previously studied in a MWL analysis that allowed us to fix some of spectral parameters. The spectrum shape was modified either by the inclusion of heavy CRs or by changing the sharpness β of the cut-off of the accelerated particle spectrum.

In the first study, the spectrum shape was changed by the inclusion of heavy CRs, in particular, CNO and Fe, for which we have taken two compositions: type II SN and GCRs composition at 1 PeV. We observed a significant softening in the spectra of the γ -ray sources which is consistent with the conclusions of [59]. For both compositions, we showed that CTAO will be able to distinguish between the γ -ray spectrum measured for protons and for protons+CNO or protons+Fe. CTAO would, therefore, help us to point back to GCR accelerators and to understand the sources responsible for the proton and Fe knee that is observed in the CR spectrum.

The diffusion of protons at the CR source has been described using different acceleration models. Different diffusion coefficients are related to the sharpness β of the particle distribution cut-off at high energies. We have performed CTAO simulations for RX J1713.7-3946 by using β values ranging from 0.50 to 1.50. The results showed that CTAO would be sensitive to a minimal change in β values of 0.10 and 0.15 considering 200 h and 50 h observation times, respectively. This sensitivity would allow CTAO to provide information on the different proton acceleration models. Furthermore, we have shown that the different shapes of the spectrum induced by heavy CRs and the change of β would allow CTAO to also distinguish between these two scenarios.

This study concerned Galactic SNRs. The CTAO Galactic Plane Survey (GPS) [60] has shown that Pulsar Wind Nebulae (PWNe) and SNRs are the two dominant Galactic γ -ray sources that would

be detected by CTAO. The survey yielded over two hundred PWNe and several tens of SNRs [61]. Therefore, CTAO has the potential to double the number of SNRs observed at TeV energies. Its high angular and energy resolution would allow us to perform detailed studies on a large number of Galactic sources and get information on the γ -ray sources of GCRs and their accelerators.

Acknowledgements

We gratefully acknowledge financial support from the agencies and organizations listed here: http://www.ctao-observatory.org/consortium_acknowledgments. This paper has gone through internal review by the CTAO Consortium.

Data Availability

This research has made use of the CTAO instrument response functions provided by the CTAO Consortium and Observatory, see <https://www.ctao-observatory.org/science/ctao-performance/> (version prod5 v0.1; [62]) for more details. Available online: <https://zenodo.org/record/5499840#.YfIV5fgRVPY>.

References

- [1] T. Antoni, W. Apel, A. Badea, K. Bekk, A. Bercuci, J. Blümer et al., *Kascade measurements of energy spectra for elemental groups of cosmic rays: Results and open problems*, *Astroparticle Physics* **24** (2005) 1.
- [2] J.R. Hörandel, *Models of the knee in the energy spectrum of cosmic rays*, *Astroparticle Physics* **21** (2004) 241.
- [3] A.M. Hillas, *Cosmic rays: Recent progress and some current questions*, 2006.
- [4] A. Aab, P. Abreu, M. Aglietta, I. Al Samarai, I.F.M. Albuquerque, I. Allekotte et al., *Observation of a large-scale anisotropy in the arrival directions of cosmic rays above 8×10^{18} eV*, *Science* **357** (2017) 1266–1270.
- [5] P. Cristofari, *The hunt for pevatrons: The case of supernova remnants*, *Universe* **7** (2021) 324.
- [6] L.O. Drury, *REVIEW ARTICLE: An introduction to the theory of diffusive shock acceleration of energetic particles in tenuous plasmas*, *Reports on Progress in Physics* **46** (1983) 973.
- [7] C. Damiano, *Understanding hadronic gamma-ray emission from supernova remnants*, *Journal of Cosmology and Astroparticle Physics* **2011** (2011) 026–026.
- [8] R.-z. Yang, E. Kafexhiu and F. Aharonian, *Exploring the shape of the γ -ray spectrum around the “ π^0 -bump”*, *Astronomy & Astrophysics* **615** (2018) A108 [1803.05072].
- [9] P. Sharma, Z. Ou, C. Henry-Cadrot, C. Dubos and T. Suomijärvi, *Multiwavelength analysis of Galactic Supernova Remnants*, *Journal of Cosmology and Astroparticle Physics* **2023** (2023) 027 [2207.02695].
- [10] F. Aharonian, A.G. Akhperjanian, A.R. Bazer-Bachi, M. Beilicke, W. Benbow, D. Berge et al., *Observations of the crab nebula with hess*, *Astronomy & Astrophysics* **457** (2006) 899–915.
- [11] J. Albert, E. Aliu, H. Anderhub, P. Antoranz, A. Armada, C. Baixeras et al., *The γ -ray observation of the crab nebula and its pulsar with the magic telescope*, *The Astrophysical Journal* **674** (2008) 1037–1055.
- [12] T. Weekes, H. Badran, S. Biller, I. Bond, S. Bradbury, J. Buckley et al., *Veritas: the very energetic radiation imaging telescope array system*, *Astroparticle Physics* **17** (2002) 221–243.
- [13] Cherenkov Telescope Array Consortium, B.S. Acharya, I. Agudo, I. Al Samarai, R. Alfaro, J. Alfaro et al., *Science with the Cherenkov Telescope Array* (2019), 10.1142/10986.

- [14] F.A. Aharonian, A.G. Akhperjanian, K.M. Aye, A.R. Bazer-Bachi, M. Beilicke, W. Benbow et al., *High-energy particle acceleration in the shell of a supernova remnant*, *Nature* **432** (2004) 75 [[astro-ph/0411533](#)].
- [15] E. Pfeffermann and B. Aschenbach, *Int. conf. x-ray astronomy and astrophysics: Röntgenstrahlung from the universe*, .
- [16] Y. Fukui, Y. Moriguchi, K. Tamura, H. Yamamoto, Y. Tawara, N. Mizuno et al., *Discovery of Interacting Molecular Gas toward the TeV Gamma-Ray Peak of the SNR G 347.3–0.5*, *Publications of the Astronomical Society of Japan* **55** (2003) L61.
- [17] H. Sano and Y. Fukui, *The interstellar medium in young supernova remnants: key to the production of cosmic x-rays and γ -rays*, *Astrophysics and Space Science* **366** (2021) .
- [18] P. Slane, B.M. Gaensler, T.M. Dame, J.P. Hughes, P.P. Plucinsky and A. Green, *Nonthermal x-ray emission from the shell-type supernova remnant g347.3–0.5*, *The Astrophysical Journal* **525** (1999) 357.
- [19] Y. Fukui, H. Sano, J. Sato, K. Torii, H. Horachi, T. Hayakawa et al., *A Detailed Study of the Molecular and Atomic Gas toward the γ -Ray Supernova Remnant RX J1713.7-3946: Spatial TeV γ -Ray and Interstellar Medium Gas Correspondence*, *Astrophysical Journal* **746** (2012) 82 [[1107.0508](#)].
- [20] F. Acero, R. Aloisio, J. Amans, E. Amato, L.A. Antonelli, C. Aramo et al., *Prospects for cherenkov telescope array observations of the young supernova remnant rx j1713.7-3946*, *The Astrophysical Journal* **840** (2017) 74.
- [21] G. Joncas and L.A. Higgs, *The DRAO galactic-plane survey. II. Field at $l=105$* , *Astronomy & Astrophysics* **82** (1990) 113.
- [22] R. Kothés, B. Uyaniker and S. Pineault, *The supernova remnant g106.3+2.7 and its pulsar-wind nebula: Relics of triggered star formation in a complex environment*, *The Astrophysical Journal* **560** (2001) 236.
- [23] Z. Cao, F.A. Aharonian, Q. An, L.X. Axikegu, Bai, Y.X. Bai, Y.W. Bao et al., *Ultrahigh-energy photons up to 1.4 petaelectronvolts from 12 γ -ray Galactic sources*, *Nature* **594** (2021) 33.
- [24] K. Fang, M. Kerr, R. Blandford, H. Fleischhack and E. Charles, *Evidence for peV proton acceleration from fermi-lat observations of snr G106.3 + 2.7*, *Phys. Rev. Lett.* **129** (2022) 071101.
- [25] V.A. Acciari, E. Aliu, T. Arlen, T. Aune, M. Bautista, M. Beilicke et al., *Detection of extended vhe gamma ray emission from g106.3+2.7 with veritas*, *The Astrophysical Journal* **703** (2009) L6–L9.
- [26] M.H. Heyer, C. Brunt, R.L. Snell, J.E. Howe, F.P. Schloerb and J.M. Carpenter, *The five college radio astronomy observatory co survey of the outer galaxy*, *The Astrophysical Journal Supplement Series* **115** (1998) 241.
- [27] G. Verna, F. Cassol, H. Costantini and C. Consortium, *HAWC J2227+610: a potential PeVatron candidate for the CTA in the northern hemisphere*, in *37th International Cosmic Ray Conference*, p. 904, Mar., 2022, DOI [[2110.07939](#)].
- [28] T. Tanaka, Y. Uchiyama, F.A. Aharonian, T. Takahashi, A. Bamba, J.S. Hiraga et al., *Study of nonthermal emission from snr rx j1713.7-3946 withsuzaku*, *The Astrophysical Journal* **685** (2008) 988–1004.
- [29] A.A. Abdo, M. Ackermann, M. Ajello, A. Allafort, L. Baldini, J. Ballet et al., *Observations of the young supernova remnant rx j1713.7-3946 with the fermi large area telescope*, *The Astrophysical Journal* **734** (2011) 28.
- [30] F. Aharonian, A.G. Akhperjanian, A.R. Bazer-Bachi, M. Beilicke, W. Benbow, D. Berge et al., *Primary particle acceleration above 100 tev in the shell-type supernova remnant rx j1713.7-3946 with deep hess observations*, *Astronomy & Astrophysics* **464** (2006) 235–243.
- [31] Y. Xin, H. Zeng, S. Liu, Y. Fan and D. Wei, *VER J2227+608: A Hadronic PeVatron Pulsar Wind Nebula?*, *The Astrophysical Journal* **885** (2019) 162 [[1907.04972](#)].

- [32] A. Albert, R. Alfaro, C. Alvarez, J.R.A. Camacho, J.C. Arteaga-Velázquez, K.P. Arunbabu et al., *Hawc j2227+610 and its association with g106.3+2.7, a new potential galactic pevatron*, *The Astrophysical Journal Letters* **896** (2020) L29.
- [33] A.M. Hillas, *The Origin of Ultra-High-Energy Cosmic Rays*, *Annual Review of Astronomy and Astrophysics* **22** (1984) 425.
- [34] K.A. Olive and Particle Data Group, *Review of Particle Physics*, *Chinese Physics C* **38** (2014) 090001.
- [35] AMS COLLABORATION collaboration, *Properties of cosmic-ray sulfur and determination of the composition of primary cosmic-ray carbon, neon, magnesium, and sulfur: Ten-year results from the alpha magnetic spectrometer*, *Phys. Rev. Lett.* **130** (2023) 211002.
- [36] J.A. Simpson, *Elemental and Isotopic Composition of the Galactic Cosmic Rays*, *Annual Review of Nuclear and Particle Science* **33** (1983) 323.
- [37] S. Thoudam, J.P. Rachen, A. van Vliet, A. Achterberg, S. Buitink, H. Falcke et al., *Cosmic-ray energy spectrum and composition up to the ankle: the case for a second galactic component*, *Astronomy & Astrophysics* **595** (2016) A33.
- [38] F.X. Timmes, S.E. Woosley and T.A. Weaver, *Galactic Chemical Evolution: Hydrogen through Zinc*, *Astrophysical Journals* **98** (1995) 617 [[astro-ph/9411003](https://arxiv.org/abs/astro-ph/9411003)].
- [39] V. Tatischeff, J.C. Raymond, J. Duprat, S. Gabici and S. Recchia, *The origin of Galactic cosmic rays as revealed by their composition*, *Monthly Notices of the Royal Astronomical Society* **508** (2021) 1321 [<https://academic.oup.com/mnras/article-pdf/508/1/1321/40509045/stab2533.pdf>].
- [40] D.C. Ellison, L.O. Drury and J. Meyer, *Galactic cosmic rays from supernova remnants. ii. shock acceleration of gas and dust*, *The Astrophysical Journal* **487** (1997) 197–217.
- [41] K. Lodders, H. Palme and H.P. Gail, *Abundances of the Elements in the Solar System*, *Landolt & Bornstein* **4B** (2009) 712 [[0901.1149](https://arxiv.org/abs/0901.1149)].
- [42] S. Gabici and F.A. Aharonian, *Hadronic gamma-rays from rx j1713.7-3946?*, *Monthly Notices of the Royal Astronomical Society: Letters* **445** (2014) L70–L73.
- [43] F.A. Aharonian and A.M. Atoyan, *On the emissivity of “ π^0 -decay” gamma radiation in the vicinity of accelerators of galactic cosmic rays.*, *Astronomy & Astrophysics* **309** (1996) 917.
- [44] S. Gabici, F.A. Aharonian and P. Blasi, *Gamma rays from molecular clouds*, *Astrophysics and Space Science* **309** (2007) 365 [[astro-ph/0610032](https://arxiv.org/abs/astro-ph/0610032)].
- [45] E.O. Angüner, G. Spengler, E. Amato and S. Casanova, *Search for the galactic accelerators of cosmic rays up to the knee with the pevatron test statistic*, *Monthly Notices of the Royal Astronomical Society* **523** (2023) 4097–4112.
- [46] A.R. Bell, *Turbulent amplification of magnetic field and diffusive shock acceleration of cosmic rays*, *Monthly Notices of the Royal Astronomical Society* **353** (2004) 550.
- [47] T. Inoue, R. Yamazaki, S. ichiro Inutsuka and Y. Fukui, *Toward understanding the cosmic-ray acceleration at young supernova remnants interacting with interstellar clouds: Possible applications to rx j1713.7-3946*, *The Astrophysical Journal* **744** (2011) 71.
- [48] V.N. Zirakashvili and F.A. Aharonian, *Nonthermal Radiation of Young Supernova Remnants: The Case of RX J1713.7-3946*, *Astrophysical Journal* **708** (2010) 965 [[0909.2285](https://arxiv.org/abs/0909.2285)].
- [49] T. Inoue, *Turbulent Magnetic Field Amplification behind Strong Shock Waves in GRB and SNR*, in *Death of Massive Stars: Supernovae and Gamma-Ray Bursts*, P. Roming, N. Kawai and E. Pian, eds., vol. 279, pp. 335–336, Sept., 2012, DOI.
- [50] C. Nigro, C. Deil, R. Zanin, T. Hassan, J. King, J.E. Ruiz et al., *Towards open and reproducible multi-instrument analysis in gamma-ray astronomy*, *Astronomy & Astrophysics* **625** (2019) A10 [[1903.06621](https://arxiv.org/abs/1903.06621)].

- [51] D. Foreman-Mackey, D.W. Hogg, D. Lang and J. Goodman, *emcee: The mcmc hammer*, *Publications of the Astronomical Society of the Pacific* **125** (2013) 306.
- [52] V. Zabalza, *naima: a python package for inference of relativistic particle energy distributions from observed nonthermal spectra*, *Proc. of International Cosmic Ray Conference 2015* (2015) 922 [[1509.03319](#)].
- [53] E. Kafexhiu, F. Aharonian, A.M. Taylor and G.S. Vila, *Parametrization of gamma-ray production cross sections for $p p$ interactions in a broad proton energy range from the kinematic threshold to PeV energies*, *Physical Review D* **90** (2014) 123014 [[1406.7369](#)].
- [54] S.R. Kelner, F.A. Aharonian and V.V. Bugayov, *Energy spectra of gamma rays, electrons, and neutrinos produced at proton-proton interactions in the very high energy regime*, *Physical Review D* **74** (2006) 034018 [[astro-ph/0606058](#)].
- [55] J.R. Letaw, *Proton production cross sections in proton-nucleus collisions p* , *Physical Review C* **28** (1983) 2178.
- [56] A. Donath, R. Terrier, Q. Remy, A. Sinha, C. Nigro, F. Pintore et al., *Gammapy: A Python package for gamma-ray astronomy*, *Astronomy & Astrophysics* **678** (2023) A157 [[2308.13584](#)].
- [57] D. Horan and S. Wakely, *Tevcat: An online catalog for tev astronomy*, .
- [58] F. James and M. Roos, *Minuit: A System for Function Minimization and Analysis of the Parameter Errors and Correlations*, *Comput. Phys. Commun.* **10** (1975) 343.
- [59] M. Breuhaus, J.A. Hinton, V. Joshi, B. Reville and H. Schoorlemmer, *Galactic gamma-ray and neutrino emission from interacting cosmic-ray nuclei*, *Astronomy & Astrophysics* **661** (2022) A72 [[2201.03984](#)].
- [60] Q. Remy, L. Tibaldo, F. Acero, M. Fiori, J. Knödlseher, B. Olmi et al., *Survey of the galactic plane with the cherenkov telescope array*, in *Proceedings of 37th International Cosmic Ray Conference — PoS(ICRC2021)*, ICRC2021, Sissa Medialab, July, 2021, [DOI](#).
- [61] C. Consortium, *Prospects for a survey of the galactic plane with the cherenkov telescope array*, 2023.
- [62] C.T.A. Observatory and C.T.A. Consortium, *CTAO Instrument Response Functions - prod5 version v0.1*, Sept., 2021. [10.5281/zenodo.5499840](#).